Volume 61
Number 41
21 May 2025
Pages 7345–7520

ChemComm

Chemical Communications

rsc.li/chemcomm

ISSN 1359-7345

ROYAL SOCIETY OF CHEMISTRY

FEATURE ARTICLE

XiaoYing Sun, Bo Li *et al.*

Current status and perspective of metal-free materials as catalysts in acetylene hydrochlorination: active site, dopant, and mechanism

ChemComm

FEATURE ARTICLE

View Article Online
View Journal | View Issue

Cite this: *Chem. Commun.*, 2025, **61**, 7368

Current status and perspective of metal-free materials as catalysts in acetylene hydrochlorination: active site, dopant, and mechanism

HuiJie Wang, LingLing Shang, BaiRan Wang, XiaoYing Sun* and Bo Li*

Acetylene hydrochlorination is one of the main catalytic routes for vinyl chloride monomer (VCM) production, in particular for coal-rich regions, with mercury or noble metal chlorides as conventional catalysts. In recent years, there is a fast-growing transition from metal-based catalysts to metal-free materials for acetylene hydrochlorination because of strict environmental regulation and strong motivation for sustainable development, and this trend is clearly exemplified in a series of studies on carbon, boron nitride, graphitic carbon nitride, and ionic liquids, which garnered significant interest as catalysts in acetylene hydrochlorination. In this review, the current status and development of these metal-free catalysts are summarized with a focus on the nature of active sites, doping effects, reaction mechanism, and optimization methods, in order to provide a timely account. For carbon materials, the essential role of nitrogen dopants in catalytic performance is elaborated and possible active nitrogen species are explored, and the dual dopant strategy is discussed in the frame of synergetic effects which could further boost the activity and stability. For the other metal-free materials, they exhibited a different pattern regarding reactant adsorption and reaction mechanism from the carbon catalysts, in particular a dual-site mechanism is found due to the balanced adsorption between HCl and C_2H_2. For each metal-free material, a short discussion is provided at the end of the section to shed light on the unique property which uncovered the difference from not only conventional metal catalysts but also the other metal-free materials. In the end, the key issues preventing the further improvements of metal-free catalysts and the practical way to replace metal catalysts are discussed. Overall, the current work paves the way for the future development of metal-free catalysts for acetylene hydrochlorination.

Received 31st December 2024,
Accepted 31st March 2025

DOI: 10.1039/d4cc06830k

rsc.li/chemcomm

Institute of Catalysis for Energy and Environment, College of Chemistry and Chemical Engineering, Shenyang Normal University, Shenyang 110034, China.
E-mail: sunxiaoying78@163.com, boli@synu.edu.cn

HuiJie Wang

Mr HuiJie Wang currently is a second year graduate at Shen-Yang Normal University under the supervision of Prof. XiaoYing Sun. His research interests are the theoretical simulation of metal-free boron nitride catalysts in propane dehydrogenation and acetylene hydrochlorination.

LingLing Shang

Ms LingLing Shang currently is a second year graduate at Shen-Yang Normal University under the supervision of Prof. Bo Li. Her research interests are the computational simulation of doped zirconia catalysts in propane dehydrogenation.

1. Introduction

Polyvinyl chloride (PVC) is produced by polymerization of the vinyl chloride monomer (VCM), which is a very important chemical polymer with an average annual production of about 30 million tons worldwide.[1–3] Due to its excellent physical and chemical properties, such as light weight and chemical resistance, PVC is the third largest widely produced synthetic plastic polymer in the world after polyethylene (PE) and polypropylene (PP). It is widely used for packaging purposes in various end-use industries such as construction industry, shrink-wrapping, drug delivery, service industry, *etc.*[4] Therefore, the development of an efficient VCM production strategy is urgently needed to meet the fast-growing demands. There are three main technological routes for PVC production, specifically acetylene hydrochlorination, vinyl dichloride coupling, and ethylene/ethane oxychlorination, as shown in Fig. 1.[3] Among these routes, ethylene oxychlorination is a petroleum-derived reaction that has been used in petroleum-rich countries for almost 70 years due to the maturity of the technology and its environmentally friendly nature. Ethane oxychlorination has also been developed since the 1960s, as ethane is considered the cheapest feedstock of all options.

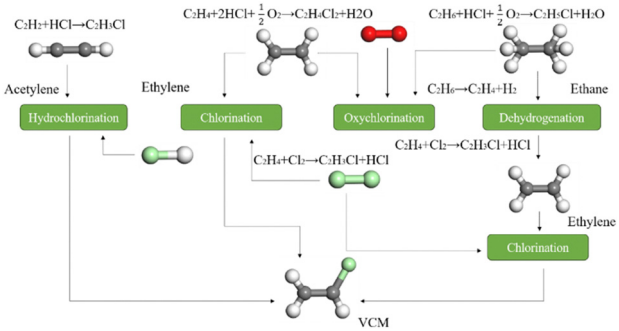

Fig. 1 Schematic illustration of various PVC synthesis routes.

Compared with other methods, acetylene hydrochlorination reaction is not only a mild process (100–200 °C), reducing the cost of equipment and energy consumption, but also the source of raw materials is flexible, therefore reducing the dependence on petrochemical raw materials, and is particularly suitable for coal rich regions.[5–7] In addition, there are fewer by-products and less pressure on environmental protection resulting from acetylene hydrochlorination, which reduces the cost of separation and is more adaptable to the current demand for the adjustment of energy structure. China's PVC production capacity was approximately 5.56×10^7 tons in 2024, of which approximately 80% of PVC production came from the acetylene hydrochlorination route, accounting for approximately 40% of global PVC production capacity.[1,3]

Mercury chloride catalysts, which are very active and selective in reaction, have been the focus for acetylene hydrochlorination over the past few decades. However, toxic and hazardous $HgCl_2$ catalysts have many drawbacks, such as hot spots in industrial fixed-bed reactors that cause sublimation

BaiRan Wang

Mr BaiRan Wang currently is a second year graduate at ShenYang Normal University under the supervision of Prof. XiaoYing Sun. His research interests are the screening of effective dual atom catalysts by machine learning.

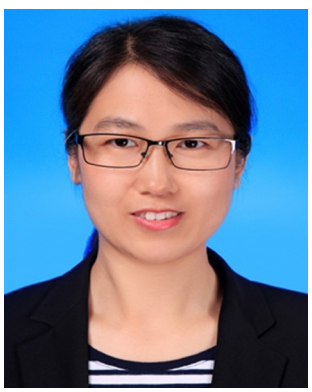

XiaoYing Sun

Prof. XiaoYing Sun received her PhD from JiLin University. After her PhD graduation, she moved to the Technical University of Berlin and joined Prof. van Wuellen's group as a Postdoc. Thereafter, she moved to the University of California, Santa Barbara, and joined Prof. Horia Metiu's group as a Postdoc. In 2013, she joined the Catalysis and Materials division of the Institute of Metal Research as a research associate. Currently, she is a professor at ShenYang Normal University. Her main research interest is to explore short alkane activation, CO_2 hydrogenation and novel electrochemistry catalysts by computational simulation.

Bo Li

Prof. Bo Li obtained his PhD degree from the Fritz Haber Institute of Max Planck Society in 2009 under the supervision of Prof. Angelos Michaelides and Prof. Mattias Scheffler. From 2009 to 2011, he was a postdoc in Prof. Metiu's group in the Chemistry Department of University of California, Santa Barbara. Currently, he is a Professor in the College of Chemistry and Chemical Engineering in ShenYang Normal University. His main research interest is computational simulation of heterogeneous catalysis including light alkane dehydrogenation, CO_2 electrochemical reduction, CO_2 hydrogenation, single atom catalysts, and Li–S battery. He has already published over 90 articles.

and loss of active mercury components, and catalyst fabrication, utilization, and disposal might cause environmental pollution.[8] The Minamata Convention, proposed by the United Nations Environment Program in 2013, has called for a ban on the use of mercury catalysts in VCM plants from 2022.[9] Therefore, exploring efficient non-mercury catalysts for acetylene hydrochlorination to achieve sustainability in the PVC supply chain is an imminent challenge.

On the other hand, the alternative metal catalysts such as gold, ruthenium, palladium, and copper have demonstrated promising activity in acetylene chlorination.[10–13] Among them, gold-based catalysts have shown extraordinarily high activity and selectivity at low temperatures, and the plant trial for acetylene hydrochlorination *via* the Au/C catalyst was realized in 2015.[14] For metal catalysts, it was found that the standard electrode potential of an active metal can be used as an activity descriptor for acetylene hydrochlorination, and AC-loaded $HAuCl_4$ was proposed as a highly active hydrochlorination catalyst by using this relation.[15,16] Recently, the service life of gold-based catalysts has been extended to 3000 hours and a pilot plant using gold catalysts has been in operation.[17] Although metal catalysts are highly active and selective in the hydrochlorination of acetylene, the direct application of metal catalysts still faces severe challenges. Firstly, the high cost of precious metals such as gold and ruthenium increases production costs. Secondly, these catalysts are susceptible to poisoning by impurities, leading to deactivation and frequent regeneration. In addition, precious metal catalysts are prone to valence changes, catalyst aggregation and deactivation during reaction, which shadowed the future of possible industrial implementation.[10–12]

In the pursuit to resolve the bottleneck issues of metal catalysts for acetylene hydrochlorination, low-cost metal-free materials appeared to be a new class of catalysts which demonstrated comparable performance to conventional metal catalysts.[18–20] Non-metallic materials including carbon materials, boron nitride (BN), graphitic boron nitride (g-C_3N_4), and ionic liquids are widely explored as alternative catalysts for acetylene hydrochlorination other than metal catalysts. In recent years, there has been a rapid development of metal-free catalysts, which demonstrate excellent conversion, selectivity, and durability. Moreover, metal-free catalysts exhibit a unique mechanism which obeys either the Langmuir–Hinshelwood (L–H) or Eley–Rideal (E–R) mechanism. As shown in Fig. 2, there is a close connection between mechanism preference and adsorption strength of reactant molecules. For the L–H mechanism, it is required that the adsorption strength of acetylene and HCl is in the mid-range and similar to each other. For the E–R mechanism, only one molecule exhibits strong adsorption and the other one is involved from the gas phase and it shows negligible adsorption.

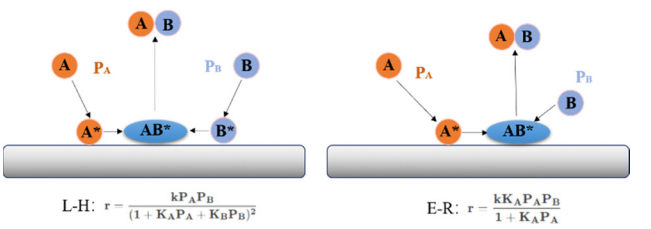

Fig. 2 Schematic diagram of the L–H and E–R mechanism and the related rate equation, where P_A and P_B are the partial pressure of A and B, and K_A and K_B are the equilibrium constants of A and B adsorption.

Overall, the proliferation of non-metallic catalysts provides a great opportunity to replace the noble metal and mercury-based catalysts used in industry, and also significantly reduces the cost and supports sustainable development. In this Feature Article, we attempt to provide a concise summary of recent advances of metal-free catalysts including carbon-based materials, boron nitride, graphitic carbon nitride, and ionic liquids for acetylene hydrochlorination with a focus on active site identification, mechanism clarification, and unique features of metal-free materials. At the end of each section, a short discussion of each investigated material is presented to reveal the differences between metal-free catalysts and the conventional metal catalysts. Although there are a few review articles in the literature which have covered some developments of VCM catalysts,[8,21–23] to the best of our knowledge, the above-mentioned aspects have not been adequately addressed in these works. Furthermore, the comparisons among metal-free materials are also made to understand the advantage and disadvantage of each material to serve as a guideline for further optimization.

2. Carbon based catalysts

2.1 Intrinsic defects on carbon catalysts

Carbon-based materials including carbon nanotubes, graphene, active carbon, and nanodiamonds have received great attention due to their unique properties such as abundant resources, high tunability, strong stability, sustainability, as well as environmental friendliness.[24] Conventionally, carbon materials were mainly used as a support for metal catalysts in acetylene hydrochlorination due to their chemical inertness and stability.[25–27] However, it takes a while to recognize that the metal-free carbon materials do exhibit remarkable activity in acetylene hydrochlorination. The observed activity is considered to have originated from the intrinsic defects such as mono-vacancy, di-vacancy, edges, Stone–Wales defects, *etc.*, as shown in Fig. 3a. The unsaturated coordination at defective sites facilitates molecular adsorption and activation. Furthermore, the well-patterned π electron network of carbon materials is broken at defective sites which causes charge redistribution and polarization, and both are conducive for molecular activation. Therefore, both geometry and electronic factors of defective sites contribute to the reactivity of carbon materials in acetylene hydrochlorination.

In one of the pioneering studies, Lan *et al.*[28] prepared a defect-rich core–shell structure with a few layer graphite shell and a nanodiamond core (ND@G), which showed a comparable performance to contemporary metal catalysts, such as Au/C and $HgCl_2$/AC catalysts, as shown in Fig. 4a. ND@G demonstrated an acetylene conversion of 50% at 220 °C and retained a stable performance with no activity decrease for 200 h as shown in

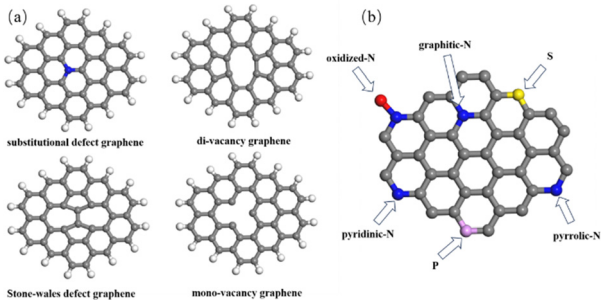

Fig. 3 Schematic illustration of (a) defects and (b) heteroatom doping configurations on carbon materials.

Fig. 4b. It is well known that I_D/I_G is an important parameter for evaluating the degree of graphitization/defects of carbon materials from Raman analysis.[29] It was found that the I_D/I_G ratio of ND@G was higher than that of both ND and OLC, which clearly indicated that there are more defects in ND@G. And also the defects are mostly located in graphite layers; hence it is concluded that the reactivity of the ND@G catalyst in acetylene hydrochlorination is mainly originated from the inherent defects of the graphite shell. In another work, a linear relationship between defect quantity and C_2H_2 conversion was established, as shown in Fig. 4c, for metal-free AC catalysts, which further corroborated the key catalytic role of defects.[30]

On the other hand, the degree of graphitization effectively affects the defective sites of carbon materials, which in turn influences the activity in acetylene hydrochlorination. The relationship between the degree of graphitization and active sites was carefully discussed by Liu *et al.*[31] They investigated four different sources of commercially available activated carbon: green-based activated carbon (PBC), coal-based activated carbon (CBC), coconut-based activated carbon (CCN), and wood-based activated carbon (WBC), and calculated the intensity ratios I_D/I_G of the different activated carbons. The results showed that the ratio of I_D/I_G decreased in the order of CBC > PBC > CCN > WBC, which is consistent with the order of activity of activated carbon. The results suggested that activated carbon with lower surface graphitization can provide more active sites, which implied that defective sites played a key role in the reaction.

Another key factor of carbon materials is the ratio between sp^2 and sp^3 hybridization, which is also an indicator of degree of graphitization which in principle will influence the catalytic performance in acetylene hydrochlorination.[32] In fact, Li's group[33] successfully identified the sp^2/sp^3 ratio as an effective descriptor for carbon catalysts in acetylene hydrochlorination and the optimal sp^2 content was determined as 32–35% which achieved the largest reaction rate as shown in Fig. 5a. The authors started from pure sp^2 graphene and sp^3 nanodiamond, and gradually increased the sp^2 and sp^3 content which resulted in a volcano curve and the peak of the curve was at the 32–35% sp^2 content. The rationale behind this observation is that an increase in either sp^2 or sp^3 carbon will cause the breaking of the regular π electron network and induce electron localization and polarization which enhances the adsorption of reactant molecules.[33]

A similar conclusion was also reached in a study of activated carbon fiber (ACF) as a catalyst for acetylene hydrochlorination. Tang *et al.*[34] prepared four ACF materials with different degrees of graphitization by impregnating them with iron salt solutions (impregnation concentrations of 0.25 mol L^{-1}, 0.75 mol L^{-1}, 1 mol L^{-1}, and 1.5 mol L^{-1}, respectively). It was found that the iron content in carbon fiber preparation has a linear relationship with graphitization degree, and more iron leads to greater graphitization. It was shown that the catalytic performance exhibits a volcano curve, *i.e.*, it increased initially and then decreased with the sp^2 content as shown in Fig. 5b, and the sample with 1 mol L^{-1} iron content showed the largest acetylene conversion. On the other hand, DFT calculations showed that C_2H_2 molecules preferred to be adsorbed at the interface between the graphene layer and activated carbon fibers, and the adsorption energy increased with increasing graphitization

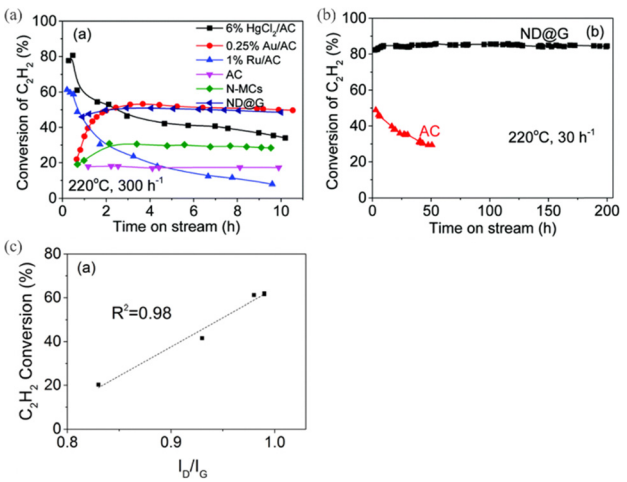

Fig. 4 (a) Conversion of acetylene for various catalysts in acetylene hydrochlorination. Temperature: 220 °C; GHSV of C_2H_2 = 300 h^{-1};[28] (b) the stability test of ND@G in acetylene hydrochlorination (220 °C, GHSV of C_2H_2 = 30 h^{-1});[28] reproduced from ref. 28 with permission from The Royal Society of Chemistry, Copyright 2019. (c) The relationship of catalytic activity of defective AC with I_D/I_G calculated from Raman spectra.[30] Reproduced from ref. 30 with permission from Elsevier, Copyright 2019.

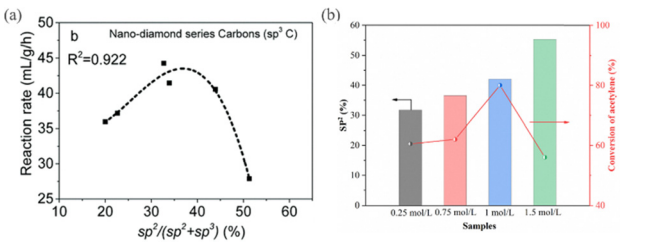

Fig. 5 (a) The relationship between the reaction rate and the sp^2 content of sp^3-oriented carbon catalysts;[33] reproduced from ref. 33 with permission from The Royal Society of Chemistry, Copyright 2020. (b) The relationship between acetylene conversion and sp^2 content. Reaction conditions: T = 180 °C, GHSV(C_2H_2) = 30 h^{-1}, V(HCl) : V(C_2H_2) = 1.2 : 1.[34] Reproduced from ref. 34 with permission from Elsevier, Copyright 2022.

degree. However, either too weak or too strong adsorption of C_2H_2 is not beneficial for catalytic performance which explained the observed volcano curve of conversion.

Although the above-mentioned experimental studies clearly pointed out the key role played by defective sites, an accurate quantitative description of interactions between defective sites and reactant molecules is still missing. Zhao *et al.*[35] carried out DFT calculations of acetylene hydrochlorination at defective sites including mono-vacancy graphene (MVG), di-vacancy graphene (DVG) and Stone–Wales defect graphene (SWDG) and made a direct comparison with the pristine counterpart at the same footing. One of the notable differences between defective sites and the pristine counterpart is that the former significantly increased the adsorption of both C_2H_2 and HCl compared with the latter case. For example, C_2H_2 adsorption was highly endothermic by 42.64 kcal mol^{-1} on pristine graphene, and it turned to be exothermic at defective sites with up to -13 kcal mol^{-1} which clearly supported the positive role of defects. From potential energy profile calculations, they also identified that HCl dissociation is the rate-limiting step and the reactivity of defective sites increased along MVG, SWDG, and DVG.

Overall, it is generally accepted that defects on carbon materials are the active sites in acetylene hydrochlorination which was verified from both experimental and computational studies. On the other hand, the precise manipulation of the kind and number of defects is still challenging, which impeded the further improvements in a controllable manner.[36,37] On the other hand, the defects number on carbon materials can be roughly estimated by the evaluation of graphitization degree or sp^2/sp^3 ratio which provide a method to control defects level in a systematical way. The possible unique reaction mechanism associated with carbon materials compared with conventional metal catalysts should be further pursued, which requires a combined experimental and computational effort. In the end, caution should be exercised while evaluating the reactivity of carbon materials as extremely low metal residues, which are very likely to be present even after careful acid washing, could significantly enhance the performance.[38]

2.2 Carbon-based catalysts doped with one element

The doping with heteroatoms such as nitrogen, boron, sulphur, and phosphorus could dramatically change the properties of carbon materials and trigger the reactivity which pure carbon materials cannot deliver.[39,40] These heteroatom dopants, in particular nitrogen, can enter the lattice of carbon materials because of similar atomic radius and induce local geometry distortion and charge polarization, which subsequently modulates the catalytic properties of carbon materials.[41] Although as described in the previous section pure carbon materials indeed have good catalytic performance in acetylene hydrochlorination, the adoption of the doping strategy further increases the performance of carbon materials; more importantly doping is an on-purpose optimization method which could potentially tune performance in a systematic way.

2.2.1 Nitrogen doping. There is no doubt that studies on nitrogen doped carbon materials are overwhelmingly more compared to the other dopants due to their wide application scope and extraordinary performance.[42–44] For example, Li *et al.*[45] tested several carbon materials, including commercial carbon black, carbon nanotubes, and ordered mesoporous carbon materials, to investigate their catalytic activity for acetylene hydrochlorination. Carbon black and nanotubes barely had any activity with an acetylene conversion of 2%, while the conversion significantly increased to 17% when introducing the nitrogen dopant as shown in Fig. 6a. The authors also recognized the importance of high surface area for this reaction; therefore the combination of nitrogen dopants and mesoporous carbon with a high surface area achieved a remarkable performance with acetylene conversion reaching 77% and vinyl chloride selectivity above 98% at a space velocity of 1.0 mL min^{-1} g^{-1} and 200 °C, which outperformed the conventional $HgCl_2$ catalysts. This work provided the convincing evidence of the positive effects of nitrogen doping for carbon catalysts in acetylene hydrochlorination. Moreover, they observed that nitrogen doping significantly increases the adsorption strength and capacity of acetylene for carbon catalysts which might be an explanation for enhanced performance.

In fact, it is often proposed that the addition of nitrogen dopants at a suitable doping level can significantly improve

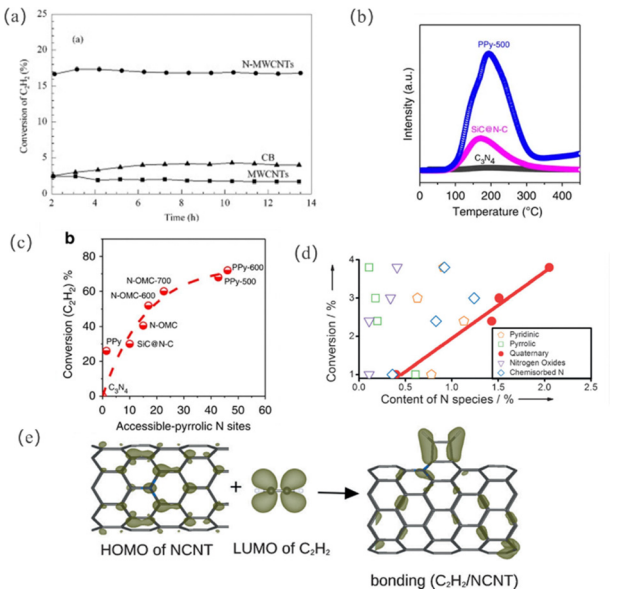

Fig. 6 (a) Comparison of the catalytic activity of CB, MWCNTs and N-MWCNTs in the hydrochlorination of acetylene at a space velocity of 3.1 mL min^{-1} g^{-1} based on the catalyst mass.[45] Reproduced from ref. 45 with permission from Elsevier, Copyright 2014. (b) TPD of acetylene on different catalysts.[46] (c) Acetylene conversion as a function of the accessible pyrrolic N sites. Reaction condition: 200 °C, 3.1 mL g^{-1} min^{-1} and HCl/C_2H_2 = 1.15/1 (volume ratio).[46] Reproduced from ref. 46 with permission from Macmillan Publishers, Copyright 2014. (d) The fitting between nitrogen species content and reactivity towards hydrochlorination.[47] (e) The charge density of the HOMO orbital of the NCNT, the LUMO orbital of C_2H_2, and the bond formed between the NCNT and C_2H_2. Carbon is gray, nitrogen is blue, and hydrogen is white. The isosurface value is 0.02 e Å.[47] Reproduced from ref. 47 with permission from Wiley-VCH Verlag GmbH & Co. KGaA, Copyright 2014.

both catalytic performance and stability of carbon catalysts in acetylene hydrochlorination; however there is an ongoing debate on the role and type of nitrogen species in the reaction partly due to the diverse configurations and co-existence of different types of nitrogen species on carbon materials as shown in Fig. 2b. To resolve this enigma, Li *et al.*[46] reported a nitrogen-doped carbon nanocomposite (SiC@N–C) derived from silicon carbide which contained 7.1% nitrogen. The catalyst showed stable performance during a 150 hour test with acetylene conversion reaching 80% and vinyl chloride selectivity over 98% at 200 °C. In the next step, the authors separately prepared two carbon catalysts, which are derived from C_3N_4 and polypyrrole (PPy) respectively, and the former catalyst contained pyridine and quaternary nitrogen while the latter had pyrrolic nitrogen. The catalytic test indicated that carbon catalysts containing pyridinic and quaternary nitrogen showed negligible acetylene adsorption as shown in Fig. 6b. In contrast, the PPy derived catalyst demonstrated an acetylene conversion twice that of SiC@N–C and strong adsorption towards acetylene, and the C_2H_2 conversion was highly dependent on the accessible pyrrolic nitrogen sites as shown in Fig. 6c, which predominantly led to the conclusion that pyrrolic nitrogen is the most active nitrogen species. The experimental observation is consistent with DFT calculations which also indicated that the carbons which are bonding with pyrrolic nitrogen are the most active sites for acetylene adsorption. Overall, this study identified that pyrrolic nitrogen is the most active nitrogen species in the reaction and the nearby carbon atoms activated by pyrrolic nitrogen are probably the active sites in the reaction. However, the computations only calculate the potential energy surface of the pyrrolic site and there is no comparison of the reaction barrier with the other nitrogen species; moreover nitrogen species on both C_3N_4 and PPy have rather different local chemical environment from SiC@N–C, therefore direct comparisons between samples derived from C_3N_4 and PPy with SiC@N–C might not be sufficient to determine the reactivity of nitrogen species, these factors might undermine the identification of the pyrrolic site. On the other hand, there is a report from Dai's group[48] which demonstrated that metal-free C_3N_4 is very active for acetylene hydrochlorination which seemed to be contradictory to Li's work.[46]

In another study, Zhou *et al.*[47] carried out a combined experimental and computational work on nitrogen doped carbon nanotubes as a catalyst in acetylene hydrochlorination, which identified that quaternary nitrogen is the active species in the reaction with good activity (TOF = 2.3×10^{-3} s^{-1}) and high selectivity (>98%). As shown in Fig. 6d, the conversion has a linear relationship with quaternary nitrogen content and does not have any clear correlation with the other nitrogen species including pyridinic and pyrrolic nitrogen. Moreover, DFT calculations revealed that nitrogen doping increased the nucleophilicity of the CNTs and thus enhanced the interactions between the HOMO of the NCNT and the low-lying LUMO of the acetylene molecule as shown in Fig. 6e which is opposite to the conventional mechanism on metal catalysts such as gold.[49]

In fact, pyridinic, pyrrolic, and quaternary nitrogen are all often identified as active species in acetylene hydrochlorination for doped carbon catalysts, which is still lacking a consensus and a general principle to describe the performance. The diversity of active sites can be probably traced back to the complexity of carbon host materials which showed difference in many aspects such as oxygen content, surface area, defect level, morphology, *etc.* Another limiting factor is that the type of nitrogen species is mainly decided by XPS analysis which is sometimes not accurate enough to yield unambiguous classification.

Aiming to resolve the puzzle of active nitrogen species and effective descriptor, Lin *et al.* proposed the two site mechanism, according to which both pyrrolic and pyridinic nitrogen are responsible for C_2H_2 and HCl adsorption respectively,[50] by using polyaniline-derived N-doped carbon as a catalyst for acetylene hydrochlorination. As reactant molecules bind at different sites, the effective diffusion of charged ions resulting from HCl dissociation is necessary for the reaction which is described by electric conductivity. Therefore, the interplay between adsorption and electric conductivity determines the catalytic performance. This hypothesis is echoed by other studies which also emphasized that cooperation between pyridinic and pyrrolic sites is responsible for adsorption of HCl and C_2H_2 molecules.[51,52]

Although nitrogen doped carbon materials exhibited comparable or even better catalytic performance than that of conventional mercury-based catalysts, the durability of nitrogen doped carbon catalysts is still not matchable with that of conventional metal catalysts. Therefore, the origin of deactivation of nitrogen doped carbon catalysts is vividly pursued and possible catalyst regeneration methods are explored. Li *et al.*[53] employed dopamine to prepare a polydopamine (PDA)/SiC nanocomposite by wrapping a layer of PDA material around the SiC substrate as a metal-free carbon catalyst applied in acetylene hydrochlorination. During the reaction, the conversion began to decrease after the initial 350 hours and decreased by 13% when reaching 1000 hours as shown in Fig. 7a. Furthermore, it is proposed that both acetylene and vinyl chloride may oligomerize and covere the active sites causing catalyst deactivation; on the other hand, it is noted that active nitrogen content did

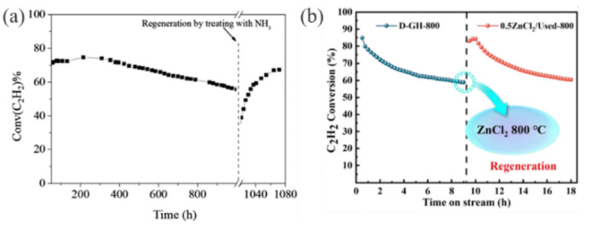

Fig. 7 (a) Stability test of PDA/SiC-700 for 1000 h and its catalytic activity upon regeneration by high temperature NH_3 treatment. Reaction conditions: 200 °C and space velocity 0.8 mL g^{-1} min^{-1}.[53] Reproduced from ref. 53 with permission from Elsevier, Copyright 2017. (b) The catalytic stability of D-GH-800 and $0.5ZnCl_2$/used-800. Reaction conditions: T = 180 °C, C_2H_2 = 180 h^{-1}, V_{HCl}/V_{C2H2} = 1.15.[54] Reproduced from ref. 54 with permission from MDPI, Copyright 2023.

not change during the reaction, suggesting that catalyst deactivation is not related to loss of active nitrogen content. Moreover, the authors realized that conventional regeneration methods such as O_2 oxidation, CO_2 oxidation, and H_2 reduction are not suitable for carbon catalysts; alternatively the catalytic performance was restored and carbon deposit was removed by NH_3 treatment as shown in Fig. 7a.

The deactivation caused by coke deposition is also verified from Lu's work, who prepared a series of nitrogen doped carbon materials by using D-glucosamine hydrochloride (D-GH), a cheap biomass material with high nitrogen content.[54] However, they propose an alternative regeneration method by using $ZnCl_2$ as they think that NH_3 treatment cannot fully remove coke and also decreases the surface area. As shown in Fig. 7b, the catalytic performance is recovered after $ZnCl_2$ treatment. More surprisingly, the surface area of the catalyst dramatically increased from 14.24 $m^2\ g^{-1}$ to 507.55 $m^2\ g^{-1}$ after regeneration. In most cases, the durability of metal-free doped carbon catalysts is around 300 h which is significantly lower than that of conventional mercury-based catalysts which showed a stable performance over 7000 h;[55] therefore it is urgent to find a new way to boost durability for carbon catalysts.

2.2.2 Other dopants. Compared to the overwhelming studies on nitrogen doped carbon catalysts, there are few reports regarding other dopants such as boron and sulfur. Boron has one less valence electron compared with carbon, which probably showed different features from nitrogen doping as nitrogen has one more valence electron compared with carbon. Yue *et al.* synthesized B-doped carbon nanodot catalysts derived from ionic liquids which mainly contained the BC_3 moiety.[56] In comparison with pristine graphene, boron doping induced positive effects as shown in Fig. 8a demonstrating an acetylene conversion of 98% at 30 h^{-1} GHSV and a space time yield (STY) of 1.19 $kg_{VCM}\ kg_{Cat}.^{-1}\ h^{-1}$ at 220 °C. Combined with DFT calculations, they identified that BC_3 is the active site in the reaction as conversion had positive correlation with BC_3 content as shown in Fig. 8b, and indicated that boron doping caused the uneven distribution of electrostatic potential which contributed to the strong adsorption of C_2H_2. It is noted that strong adsorption of C_2H_2 is also widely found on nitrogen doped carbon catalysts. However, the mechanism of C_2H_2 adsorption should be different for boron and nitrogen doped cases due to their distinct doping effects, which needs further investigations.

In another work from the same group, a carbon supported sulfur quantum dot was prepared as a catalyst for acetylene hydrochlorination by using a novel nano digging technique.[57] The optimal treatment temperature was identified as 600 °C (SC-600) which led to the most abundance of S–S bonding species of 32.6% in the investigated samples from the combined characterization of quasi-*in situ* XPS, DRIFTS, and XANES. The authors carefully evaluated the influence of reaction temperature and space velocity, and concluded that the catalyst demonstrated excellent stability at a reaction temperature of 180 °C and a GHSV of 225 h^{-1}, maintaining around 35% conversion over 300 h of reaction, with vinyl chloride selectivity

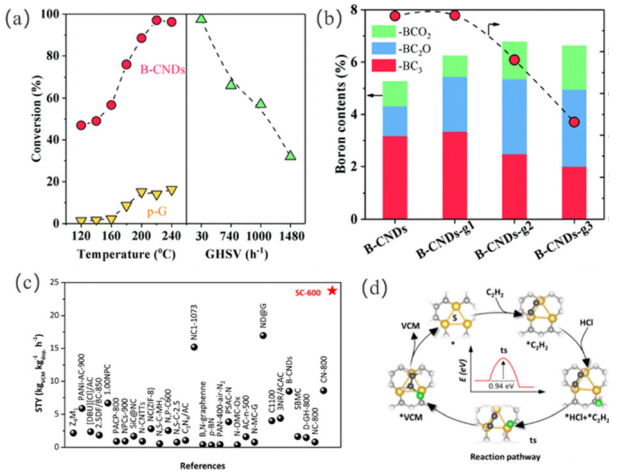

Fig. 8 (a) Conversion of acetylene over B-CNDs and pristine graphene (p-G) at different reaction temperatures and GHSV.[56] (b) The relation between conversion and specific B content estimated from XPS.[56] Reproduced from ref. 56 with permission from The Royal Society of Chemistry, Copyright 2020. (c) Comparison of the STY of acetylene hydrochlorination catalyzed by SC-600 and reference metal free catalysts.[57] (d) Reaction pathway of acetylene hydrochlorination over S-QDs.[57] Reproduced from ref. 57 with permission from American Chemical Society, Copyright 2024.

above 98%. Moreover, the obtained STY of SC-600 was determined to be 23.74 $kg_{VCM}\ kg_{Cat}.^{-1}\ h^{-1}$ which was much higher than that of the contemporary catalysts as shown in Fig. 8c. Interestingly, it was found that the catalytic performance was mainly determined by S–S content besides surface area, defect level, sulfur amount *etc.* To further corroborate this key factor, an active site model was constructed as shown in Fig. 8d and applied in DFT calculations. It was revealed that C_2H_2 is strongly bound at the S–S site and the reaction obeys the L–H mechanism with a barrier of 0.94 eV. This study uncovered a novel configuration of active sites on metal-free carbon catalysts which purely consisted of dopants and seemed to not involve adjacent carbon atoms.

In another sulfur doped carbon catalyst study, Qi *et al.*[58] proposed that the S–C site is the active center in acetylene hydrochlorination. They prepared a series of sulfur-doped spherical activated carbon (SAC) catalysts with phenyl disulfide as a sulfur source and identified that the catalyst containing 9% S (9% S/B-SAC) has the best performance, which achieved 35% conversion at a temperature of 180 °C and a GHSV of 90 h^{-1}. From XPS analysis, C–S–C was identified as the main bonding configuration for sulfur. On the other hand, DFT calculations showed that the C–S configuration at the edge induced a visible spin density which is conducive for the observed activity.

From the above discussions, several interesting observations can be made for metal-free doped carbon catalysts which might serve as a guideline for further optimization. First of all, the improvements induced by doping are substantial which not only increase the activity of carbon catalysts but also make it competitive with the conventional metal catalysts. Therefore, the doping strategy is indeed an effective method for carbon materials which justified the further developments. On the

Table 1 The survey of key information of various metal-free catalysts together with typical metal catalysts. *C*: conversion. *S*: selectivity. *T*: temperature

Year	Catalyst	*S* %	*C* %	*T*/°C	Stability/h	GHSV h^{-1}	*V*(HCl)/ *V*(C_2H_2)	Dopant content/%	Active species	Ref.
Nitrogen doped carbon catalysts										
2024	CN-800	99	81.6	180	90	90		10.29	Pyridinic N pyrrolic N	59
2023	D-GH-800		99	180	60	180	1.15	6.28	Pyridinic N	54
2023	NPCs-900	99	90.86	180	76	30	1.15	2.93	Pyrrolic N pyridinic N^+O^-	60
2023	cCTN-700	98	99	200	50	40	1.2	11.3	Pyridinic N	61
2022	1.00NPC		81	220	100	60	1.2	13.5	Pyridinic N pyrrolic N	62
2021	MPF-800	99	70	180	200	30	1.15	45.17	Pyridinic N	63
2021	NC-800		98	220	450	30		13.46	Pyridinic N pyrrolic N	64
2021	N@CBC-FE		75	220	120	180		4.81		65
2020	P-NC-1173-A6V12		81	353	25	315	1.1	3.43	Pyridinic N pyrrolic N	66
2020	SBMC-600	98	95	200	110	50	1.15	6.9	Pyrrolic N	67
2020	NC-800-700	99	97.85	220	50	83.25	1.15	13.55	Pyridinic N	68
2020	NC-III		62	250	60	650	1.1	17	Pyridinic N pyrrolic N	44
2020	CN-2	99	98	220	50	50		9.74	Pyrrolic N	69
2020	HMT	99	60	220		30		25	Single tertiary amine N	70
2019	MF-600	99	94.5	180	30	30		2.44		71
2019	PAN-400-N2	99	93	280	200	120		18.5	Pyridinic N	72
2019	3NR/4CAC		97.9	220	200	30	1.2	3.4	Pyridinic N pyrrolic N	18
2018	C1100	99	95.4	220	14	36		2.35		43
2018	NPC-800		90.72	180	8.25	63.75	0.88	2.50	Pyridinic N pyrrolic N	19
2017	N-MC	99	85.5	220	100	30		4.2	Graphitic N	73
2017	17% ZIF-8/SAC	99	81	200	500	30		1.1	Pyridinic N	42
2017	NS-C-NH_3	100	80	220	100	195	1.2	17.8	Pyrrolic N	20
2017	NC1-1073	100	81	573	100	195	1.2	7.3	Pyrrolic N	50
2016	N-OMC-O	99	33.5	180	200		1.1	3.6	Quaternary N	74
2014	SiC@N–C	98	80	200	150	30	1.15	7.1	Pyrrolic N	46
2014	PSAC-N		68	250	160	120	1.15	4.9	Pyridinic N	75
2013	g-C_3N_4/AC		76.52	180		50		8.64	Pyridinic N	76
Other metal-free catalysts										
2022	1.5ACF		95	180	12	30	1.2			34
2022	ND900	98	90	220	10	30	1.15			77
2022	[DBU][Cl]/AC	99.5	86.8	240	200	30	1.2			78
2020	SBM	98	99	110	200	30	1.2			79
2020	B-CNDs		98		220	30				80
2019	CBC		31	180	180	180	1.1			31
2019	D-AC-M		60	220	100	30	1.2			30
2018	IL/CaX	95	90	320	5	100	1.2			81
2018	1-Alkyl-3-methy limidazolium ILs	96	45	180		40	1.1–1.2			82
2018	15% TPPB/SAC	99.5	97.1	220	300	30	1.15			83
2018	ND@G	99.5	51.2	220	10	300				28
2017	p-BN	99	99	280	1000	44	1.2			84
Metal catalysts										
2019	Au-IL/SAC	100	90	170	200	360	1.2			85
2017	AC/$HgCl_2$	90	99	180	7000	1000	1.1			86
2015	Au/NAC1	99	99	180	300	1480	1.2			49
1985	$HgCl_2$	99	86	180	2880	2096	1.1			87

other hand, the unambiguous identification of active sites and accurate understanding of the reaction mechanism are the prerequisites for a rational optimization of the doping strategy; unfortunately both are not fully resolved for doped carbon catalysts as indicated in Table 1. For the identification of active dopant species, the difficulties are partly due to the interplay among several key factors including surface area, oxygen groups, defects, and morphology which wielded a paramount influence on the catalytic properties of nitrogen species. It is very challenging to filter out these influences to capture the intrinsic effects of the dopant. The coexistence of diverse nitrogen species, such as pyrrolic, graphitic, and pyridinic, is considered another hurdle for the identification of active sites due to the limitation of current characterization techniques to discern their subtle difference. The mechanisms associated with acetylene hydrochlorination catalyzed by doped carbon catalysts are mainly either L–H or E–R, and the latter is more dominant. It is noted that the adsorption of C_2H_2 seemed to be the first step in the reaction pathway to initiate the reaction because of its strong adsorption over HCl in most studies. However, the determination of the favorable mechanism still lacks convincing proof and needs more decisive factors for confirmation. Furthermore, most studies concluded that dopants increased the adsorption of reactants (C_2H_2 or HCl); however in many cases, reactant adsorption is not the rate-limiting step in the pathway, which weakened the validity of

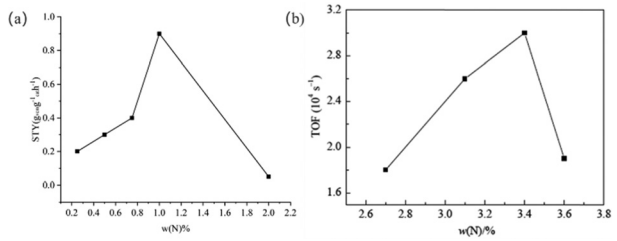

Fig. 9 (a) Space time yield of VCM of *x*NPCs with various ratios of melamine and PVC (*x* = 0.25, 0.50, 0.75, 1.00, 2.00). The reaction conditions were 220 °C, GHSV of C_2H_2 = 60 h^{-1}, HCl/C_2H_2 volume ratio = 1.2;[62] reproduced from ref. 62 with permission from American Chemical Society, Copyright 2022. (b) The relationship between nitrogen content and TOF of N-OMC-Ox.[74] Reproduced from ref. 74 with permission from Elsevier, Copyright 2016.

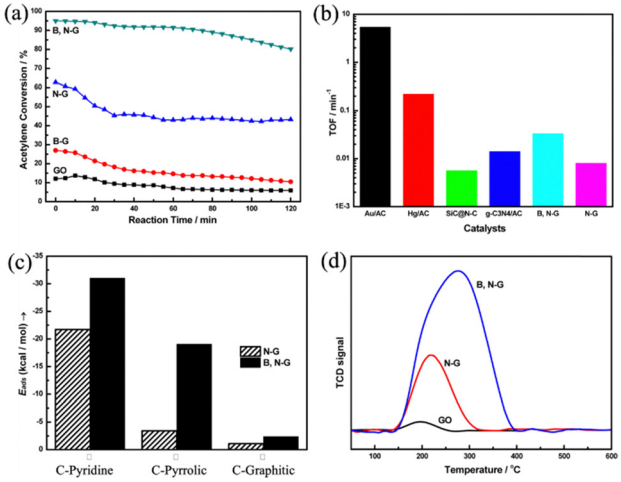

Fig. 10 (a) Catalytic reactivity evaluation of GO, B–G, N–G and B, N–G. The reactions were carried out at 150 °C, atmospheric pressure, a gas hourly space velocity (GHSV) of 36 h^{-1}, HCl/C_2H_2 = 1.15/1 (volume ratio). (b) The TOFs for different catalysts: Au/AC, Hg/AC, SiC@N–C, g-C_3N_4/AC, B, N–G, N–G. (c) E_{ads} of HCl on different types of active sites in N–G and B, N–G. C-pyridine: the carbon atoms bonded with pyridinic N species. C-pyrrolic: the carbon atoms bonded with pyrrolic N species. C-graphitic: the carbon atoms bonded with graphitic N species. (d) TPD profile of HCl on GO, N–G and B, N–G.[90] Reproduced from ref. 90 with permission from American Chemical Society. Copyright 2015.

promotional effects from the dopant. In the end, there is still a lack of a relationship or descriptor linking the intrinsic properties of dopants to the observed catalytic performance, which has severely hampered the rationale design and further improvements.

It is also noted that dopants are not always beneficial to the performance and stability. The studies from Li's group found that the performance (conversion or TOF) does not monotonously increase with increasing nitrogen content, but shows a volcano-like curve as shown in Fig. 9.[62,74] Too much nitrogen content will result in the collapse of the active structure and reduced surface area, which leads to weak interaction with reactants and a decrease of activity.

2.3 Carbon-based catalysts doped with two elements

Although single-element doping significantly enhanced the catalytic performance of carbon catalysts, this strategy sometimes also suffered the constrain of linear relationship between adsorption energy and conversion because the single dopant has limited flexibility to widely adjust the energetics of intermediates in the reaction.[88] Therefore, the dual element doping strategy is proposed to circumvent this obstacle and further increase the performance of doped carbon catalysts. In fact, the dual element doping strategy has been widely applied in electrochemistry for carbon catalysts and has shown performance which is much more pronounced than the sum of corresponding two single element doping.[89] The enhancements induced by dual atom doping are often attributed to the synergetic effects from interactions between two dopants. Therefore, dual element doping is soon recognized as an effective method to further boost the catalytic performance of carbon catalysts in acetylene hydrochlorination.

Dai *et al.*[90] prepared N and B co-doped graphene (B, N–G) catalysts and applied them in acetylene hydrochlorination together with the comparison with single element doping (B–G and N–G) under the same reaction conditions. The measured acetylene conversion clearly indicated the better performance of the B, N–G catalyst over the counterparts of single element doping as 94.98% conversion was found for B, N–G, while it was only 26.96% and 62.74% respectively for B–G and N–G catalysts as shown in Fig. 10a. The comparison undoubtedly proved the effectiveness of the co-doping strategy; moreover the B, N–G catalyst also showed a better performance than the other metal-free catalysts regarding TOF although it is still less active compared with conventional metal catalysts as shown in Fig. 10b. More importantly, the authors deduced that nitrogen is responsible for HCl adsorption and boron promoted the reactivity of nitrogen, in particular for pyrrolic type which has no obvious HCl adsorption in the N–G catalyst and was changed to be active in the B, N–G catalyst as shown in Fig. 10c. The analysis supported that the synergetic effects between nitrogen and boron are responsible for the increased performance to some extent. Moreover, the authors concluded that B, N–G has the most strong adsorption capacity for HCl molecules; since HCl adsorption is deemed to be the rate-limiting step in the reaction, it explained the origin of the superior performance as shown in Fig. 10d. Unfortunately, coke deposition caused a rapid decline of conversion which decreased from 94.89% to 61.88% within 4 h on the B, N–G catalyst. It is also noted that B, N–G still lags behind Hg and Au catalysts in terms of performance measured by TOF. In the following work from the same group, they further tested a nitrogen and sulfur co-doped carbon catalyst and found that the catalyst demonstrated an acetylene conversion of 82.44% which is retained up to 10 h without any changes. In contrast to previous work, they concluded that introduction of sulfur increased the adsorption strength of C_2H_2, and consequently improved the catalytic performance compared with the only nitrogen doped catalyst.[91]

In another sulfur and nitrogen co-doped case, Dong *et al.* explored a nitrogen and sulfur doped mesoporous carbon

catalyst in acetylene hydrochlorination.[92] First of all, the co-doped catalyst showed much improved acetylene conversion than the single nitrogen or sulfur doped catalyst; in particular the sulfur-only doped carbon catalyst showed negligible activity, which indicated that sulfur cannot be the active species. They concluded that the positive effect from sulfur doping is an increase in the proportion of active pyridinic nitrogen in the catalyst and that the carbon adjacent to pyridinic nitrogen is the active site for C_2H_2 adsorption and activation. Moreover, the co-doped carbon catalyst demonstrated stable acetylene conversion over 90% for 100 h.

In another dual element doping study, Zhao *et al.*[93] prepared a novel highly active nitrogen–phosphorus co-doped carbon-based catalyst (NP-C600) with as high as 99.2% conversion at a GHSV of 200 h^{-1} which is a relevant condition for industrial implementation, and also exhibited a stable performance for 400 hours, which is comparable to that of some well-established gold-based catalysts, and much higher than conventional mercury catalysts as shown in Fig. 11a. Although doped carbon catalysts showed tremendous potential in acetylene hydrochlorination, the performance of carbon catalysts in terms of STY is still not good enough compared with contemporary metal catalysts; however NP-C600 demonstrated an excellent STY which is very close to that of metal catalysts as shown in Fig. 11b. Furthermore, the authors also designed two separate experiments in order to identify the possible mechanism as shown in Fig. 11c. In the first experiment the catalyst was pretreated with HCl for one hour and then C_2H_2 was flowed in; however there was no VCM formation found in this setup. On the other hand, when the catalyst was pretreated with C_2H_2 firstly followed by the addition of HCl afterwards, VCM was immediately detected in the reactor. The observation from the controlled experiments suggested that the reaction obeys the E–R mechanism. Combined with DFT calculations, the active site was determined to be the *ortho*-position site with a P–N bond as shown in Fig. 11d and the rate limiting step was identified to be acetylene adsorption with a barrier of 91.83 kJ mol^{-1} which is also close to the experimentally measured activation energy of 103.47 kJ mol^{-1}.

From the above discussions, the co-doping strategy for carbon catalysts in acetylene hydrochlorination is mainly to tune the catalytic properties of nitrogen by introducing the second dopant. The so-called synergetic effects between dopants are manifested to improve the adsorption of C_2H_2 or HCl which consequently increased the catalytic performance as reactant adsorption is identified as the rate-limiting step in most cases.

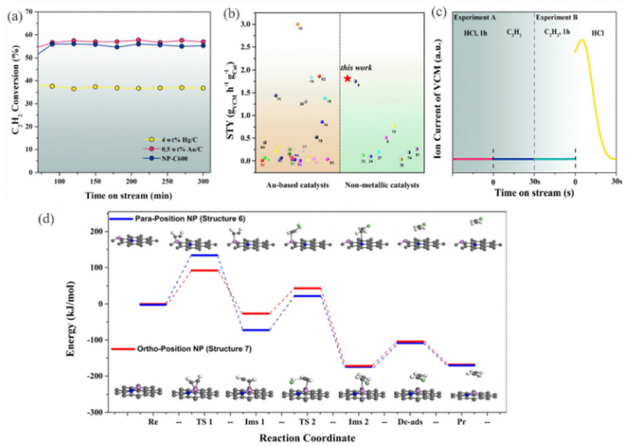

Fig. 11 (a) Conversion of acetylene over NP-C600, 0.5 wt% Au/C, and 4 wt% Hg/C catalysts. The reactions were carried out at 210 °C, space velocity GHSV(C_2H_2) of 200 h^{-1}, and HCl/C_2H_2 = 1.2/1.[93] (b) The calculated STY (g_{VCM} h^{-1} g^{-1}_{Cat}) values of NP-C600 and other catalyst materials. In all cases, the STY was calculated at a yield level of VCM < 15%.[93] (c) MS signals of VCM. Experimental A sequences: HCl, 1 h → N_2, 1 h → C_2H_2. Experimental B sequences: C_2H_2, 1 h → N_2, 1 h → HCl.[93] (d) Reaction pathway from DFT calculation for N–P doped carbon catalysts. The reactions were carried out at 210 °C and space velocity GHSV(C_2H_2) of 200 h^{-1}.[93] Reproduced from ref. 93 with permission from Elsevier. Copyright 2019.

3. Boron nitride based catalysts

Compared with carbon-based catalysts, boron nitride catalysts have been less studied in acetylene hydrochlorination reactions. However, boron nitride already stands out as a novel metal-free catalyst in heterogeneous catalytic processes such as oxidative dehydrogenation, and exhibits better performance than conventional metal oxide catalysts.[94–98] Therefore, the great potential of boron nitride in acetylene hydrochlorination can be envisioned. Li *et al.*[84] prepared porous boron nitride (p-BN) materials by treating a mixture of boric acid and melamine in NH_3 at 800 °C. At 280 °C, V_{HCl}/V_{C2H2} = 1.2, and GHSV = 1.32 mL min^{-1} g^{-1}, they found that the conversion of acetylene was as high as 99%, and the selectivity to VCM reached 99%. In contrast, no acetylene conversion was detected over the commercially available h-BN under the same conditions. Moreover, p-BN catalysts also demonstrated 81% conversion with a selectivity over 99% which is comparable with the Au catalyst under a GHSV of 120 h^{-1}, and retained a conversion of 95% for 1000 hours on stream as shown in Fig. 12a; even regenerated catalysts still showed an initial conversion of 87%. Clearly, p-BN demonstrated extraordinary catalytic performance which not only exceeded the performance of carbon-based metal free catalysts but was also comparable to that of the state-of-the-art metal catalysts. From TEM analysis, the layer distance of p-BN fell in the range of 0.35–0.40 nm and was greater than the typical 0.35 nm of commercial h-BN, which is probably due to the presence of defects. Furthermore, both carbon and oxygen contents in p-BN did not influence the catalytic performance as the conversion remained nearly unchanged with increasing carbon, and there was even loss of activity after oxidation treatment. Therefore, defective sites might be responsible for the observed performance which is supported by DFT calculations as shown in Fig. 12c. The C_2H_2 adsorption at the edge site is exothermic by 0.17 eV; however p-BN has almost no activity for HCl adsorption. The different adsorption ability of two reactant molecules rendered an E–R mechanism which is corroborated from the relation between HCl partial pressure and conversion as shown in Fig. 12b. This pioneering work

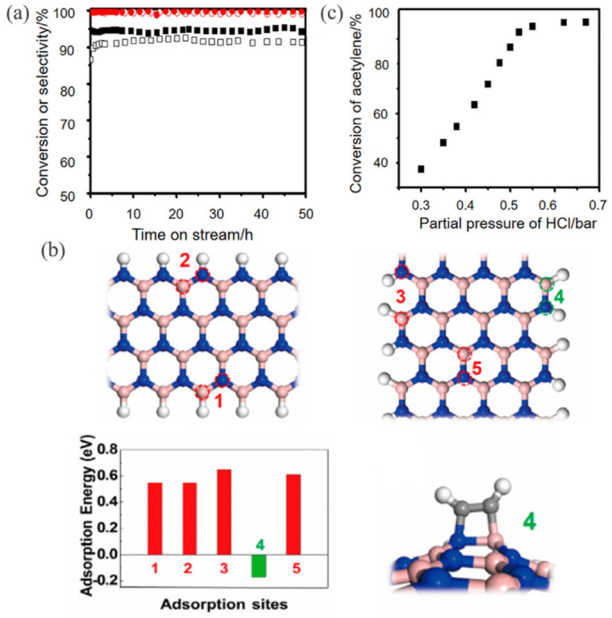

Fig. 12 (a) Stability test around 1000 h under optimized reaction conditions: 1.0 g catalyst, GHSV = 1.32 mL min^{-1} g^{-1}, HCl/C_2H_2 = 1.2, and 280 °C. (b) HCl partial pressures, with the total pressure fixed at 1.0 bar. (c) Adsorption energies and configurations at different sites.[84] Reproduced from ref. 84 with permission from American Chemical Society. Copyright 2017.

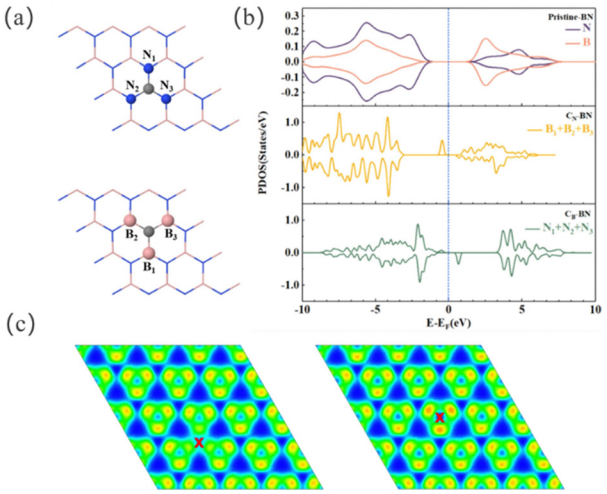

Fig. 13 Model of carbon doped h-BN, PDOS and electron localization function (ELF) plots. (a) Geometry of C-doped BN, (b) PDOS of pristine BN, CB–BN and CN–BN, (c) ELF of C-doped BN. The left is CB–BN and the right is CN–BN. The red cross indicates the position of the carbon dopant.[100] Reproduced from ref. 100 with permission from Elsevier, Copyright 2021.

clearly indicated the great potential of metal-free boron nitride materials in acetylene hydrochlorination and triggered the further investigations on boron nitride. However, the favorable adsorption of C_2H_2 is not sufficient to determine active sites unless adsorption is identified to be the rate-limiting step.

The excellent catalytic performance of metal-free boron nitride catalysts led to intensive interest in computational simulations to explore the possible further optimization strategy which is mainly attributed to replacing boron or nitrogen by carbon. In fact, carbon doping is a widely adopted strategy to activate the boron nitride catalysts which has been used in various heterogeneous catalytic processes.[99] The rationale behind this method is that carbon can easily enter the boron nitride lattice due to the similar radius and induce charge redistribution and therefore create the active site for adsorption. As shown in our previous work,[100] carbon substitution at either the boron vacancy or the nitrogen vacancy caused charge polarization and a new state appeared within the bandgap as revealed from ELF and DOS analysis as shown in Fig. 13, and both are conducive to increase reactivity. This effect is clearly indicated from C_2H_2 adsorption as the adsorption energy was exothermic by around −0.3 eV on carbon doped BN while it became highly endothermic with up to 1.27 eV on pristine BN. Moreover, five reaction pathways initiated by either C_2H_2 or HCl adsorption are investigated at the same footing and TOF calculations based on the energy span model identified that the reaction obeyed the E–R mechanism and the BN with carbon substitution at the boron site is the most active catalyst.

In another DFT investigation, Wang *et al.* explored a series of carbon doped armchair (*n*, *n*) terminated BN nanotubes (*n* = 3, 4, 6, 8) as a catalyst in acetylene hydrochlorination.[101] First of all, carbon doping significantly reduced the band gap from around 4.5 eV down to below 1 eV, which consequently increased the reactivity of BN nanotubes. It is also found that carbon doping also changed the adsorption preference for C_2H_2 and HCl: both molecules have comparable weak adsorption energies between −6.30 and −8.10 kcal mol^{-1} on the pristine BN nanotube; however the adsorption energy of C_2H_2 on the carbon doped nanotube became at least two times greater than the adsorption energy of HCl. Moreover, the active site to bind C_2H_2 is determined to be the carbon dopant rather than either boron or nitrogen. Therefore, the reaction started with the adsorption of C_2H_2 and there is only one transition state in the reaction pathway which is Cl from HCl dissociation attached to the adsorbed C_2H_2. It is noted that barriers on all investigated nanotubes are quite close to each other and the difference is within 3 kcal mol^{-1} which seemed to suggest that the curvature effect is not significant.

The promotional effects induced by carbon doping are also revealed from Zhao's DFT investigations which explore both undoped $B_{12}N_{12}$ and carbon-doped BN fullerene ($B_{12-n}N_{11+n}C$ (*n* = 0, 1)).[102] As expected, carbon doping greatly increased the adsorption of both C_2H_2 and HCl compared with the undoped case. Moreover, they examined both *trans*- and *cis*-configurations of adsorbed C_2H_2 which showed a similar adsorption energy around −28 kcal mol^{-1}. Similar to the conclusion from the BN nanotube, the active site to bind C_2H_2 is the carbon dopant itself which showed a different feature from nitrogen doped carbon materials. The most favorable pathway also involved only one transition state which is H attached to adsorbed C_2H_2 with a barrier of 36.08 kcal mol^{-1}.

From the above discussion, the barrier of rate-limiting step on pathway is in a increasing order from the nanosheet (14.53 kcal mol^{-1}), nanotube (28.47 kcal mol^{-1}), to fullerene (36.08 kcal mol^{-1}). A shared feature of three BN materials is that the carbon dopant is identified as an active site to bind C_2H_2 which showed different feature from the nitrogen dopant for carbon materials, where nitrogen is to activate neighboring carbon to bind C_2H_2. Moreover, stronger adsorption of C_2H_2 over HCl leads to the E–R mechanism for all investigated BN materials. Unfortunately, all DFT calculations did not consider the side reaction and hence have limited ability to explain the observed excellent durability. Overall, DFT calculations clearly revealed the great potential of metal-free BN materials as catalysts for acetylene hydrochlorination and provided important insight into active sites and the reaction mechanism which served as a solid ground for further experimental exploration.

4. Graphitic carbon nitride

Graphitic carbon nitride (g-C_3N_4) catalysts exhibit excellent catalytic performance in acetylene hydrochlorination, mainly due to their structural and electronic properties.[103,104] Compared with previously discussed nitrogen doped carbon materials, C_3N_4 has a more ordered structure with high nitrogen density and higher surface area, which in principle enables it to provide more active sites, and consequently enhances the catalytic activity. Compared with other catalysts, C_3N_4 exhibits excellent stability, which can maintain high catalytic activity in long-term reactions, avoiding degradation of the surface structure.

Dai *et al.*[76] prepared g-C_3N_4/AC catalysts using AC as the carrier and cyanamide as the precursor by an incipient wetness technique, and varied the cyanamide amount from 0.2 g to 0.7 g to result in a series of catalysts with different nitrogen contents. The pure g-C_3N_4 did not show any reactivity in the reaction due to low surface area. In contrast, well-tuned g-C_3N_4/AC delivered an acetylene conversion of 76.52%, although it is still less favorable compared with Au or Hg; however the reduced cost of the metal-free catalyst is still a good option for further development. It is also noted that the conversion has a good linear relationship with nitrogen content as shown in Fig. 14a and the optimal nitrogen content is determined to be 0.6 g. Moreover, g-C_3N_4 demonstrated a strong binding of HCl which is rarely observed on other metal-free catalysts and the reaction was initiated by HCl adsorption. The largest barrier along the reaction pathway is calculated to be 77.94 kcal mol^{-1} as shown in Fig. 14b.

Qiao *et al.*[71] developed a novel method to synthesize fragmented g-C_3N_4 skeletons with nitrogen-rich defects and a porous structure using melamine formaldehyde (MF) resin as an oxygen-containing precursor. A series of catalysts denoted as MF-*x* were treated at different temperatures, with *x* representing the corresponding temperature. From TEM analysis, MF-*x* showed an irregular pattern when treated above 500 °C which implied that a porous structure is achieved. The increased surface area is another indicator of porous structure formation

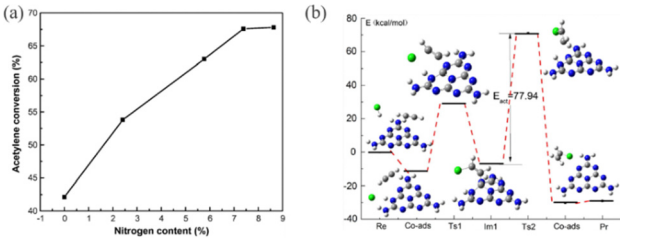

Fig. 14 (a) Effect of the nitrogen content of the g-C_3N_4/AC catalysts on acetylene conversion.[76] (b) Reaction energy diagram of the substances involved in the reaction path: reactant (Re), co-adsorbed reactants or products (Co-ads), transition state (TS), intermediate product (Im), product (Pr). Chlorine, nitrogen, carbon, and hydrogen atoms are depicted in green, blue, gray and white, respectively.[76] Reproduced from ref. 76 with permission from Elsevier, Copyright 2014.

as it rapidly increased to 161.2 m^2 g^{-1} at 800 °C, while it is below 20 m^2 g^{-1} under 550 °C. The increasing treatment temperature gradually ruptured the structure of g-C_3N_4 and more defective sites, mainly nitrogen, were exposed as revealed from XPS and Raman spectroscopy. MF-*x*, where *x* = 400, 500, and 550, have a poor activity with an acetylene conversion of 7.3%, 20.5%, and 23.4%, while the activity reached 94.5%, 97.3%, and 95.1% for MF-600, MF-700, and MF-800; hence this clearly indicated the importance of defective nitrogen sites as more nitrogen are exposed with increasing temperature in particularly above 550 °C. Moreover, MF-600 exhibited 0.35 g_{VCM} h^{-1} $g_{Cat}{}^{-1}$ STY of VCM and delivered 40 h stable performance which is comparable with other reported metal-free catalysts. The key role of nitrogen defects is also uncovered from DFT calculations and the barrier of the rate-limiting step is calculated to be 38.1 kcal mol^{-1} on the defective nitrogen site while it became 62.0 kcal mol^{-1} on pristine g-C_3N_4.

Although there are fewer reports regarding g-C_3N_4 compared with other metal-free catalysts, the great potential of g-C_3N_4 in acetylene hydrochlorination has been clearly revealed due to its large surface area, rich nitrogen content, and versatile optimization methods which rendered the unique catalytic properties such as strong binding of HCl. Moreover, g-C_3N_4 demonstrated a remarkable photocatalytic performance which potentially overcame the limitation of the conventional thermal catalytic route.

5. Ionic liquid catalysts

Ionic liquids (ILs) possess unique physicochemical properties involving high solubility, high thermal stability, and negligible volatility, and have been applied in many fields including catalysis, adsorption and organic synthesis.[105–107] The good solubility of some ILs for HCl is definitely a bonus for acetylene hydrochlorination reactions.[105,108] However, the disadvantages of ionic liquids such as high cost, operational complexity, and possible environmental risks compared to other non-metallic catalysts also limit their use in some industrial applications.

Zhou *et al.*[82] prepared a series of imidazolium-based ILs as one-component metal-free catalysts for the hydrochlorination of acetylene. Firstly, the alkyl substituents in the imidazole

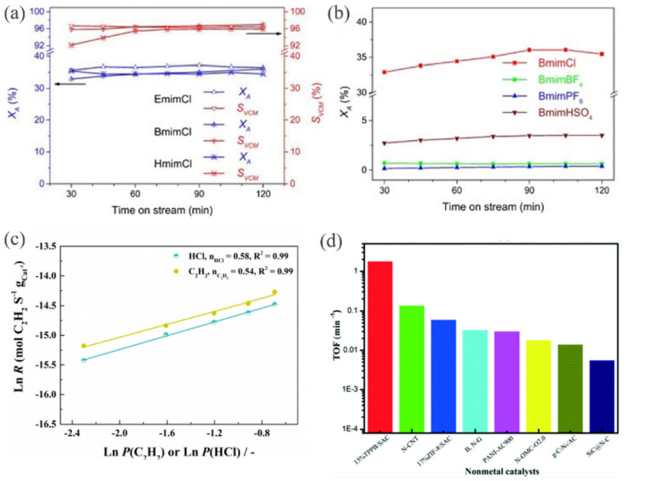

Fig. 15 (a) Effect of the substituent group in the imidazolium cation on acetylene hydrochlorination as a function of time on stream. Reaction condition: catalyst, 10 mL; reaction temperature, 180 °C; GHSV of C_2H_2, 40 h^{-1}; $V_{(HCl)}/V_{(C2H2)}$ = 1.1–1.2.[82] (b) Effect of anion species on the catalytic activity. Reaction condition: ILs, 10 mL; reaction temperature, 180 °C; GHSV of C_2H_2 40 h^{-1}; $V_{(HCl)}/V_{(C2H2)}$ = 1.1–1.2.[82] Reproduced from ref. 82 with permission from Elsevier, Copyright 2018. (c) Reaction orders for HCl and C_2H_2 over IL/CaX (calculated at <15% conversion of acetylene).[81] Reproduced from ref. 81 with permission from MDPI, Copyright 2018. (d) The TOFs for different nonmetal catalysts.[83] Reproduced from ref. 83 with permission from The Royal Society of Chemistry, Copyright 2019.

cation (Im^+) were changed from butyl to ethyl and hexyl, and the results showed that the performance is basically the same with the acetylene conversion about 35–37% and the VCM selectivity about 96% as shown in Fig. 15a; therefore the alkyl group has minimal effects on catalytic performance. Meanwhile, four anions ([Bmim]Br, [Bmim]BF_4, [Bmim]PF_6, and [Bmim]H_2SO_4) were compared as shown in Fig. 15b, and it was found that the halogen anions possessed a better catalytic activity. The results suggested that the molecule C_2H_2 located on the imidazole ring was successfully introduced into the intermediate through the strong hydrogen bonding of the anion and the π–π interaction of the imidazole ring. On the other hand, theoretical calculations have shown that ionic liquids as catalysts for the hydrochlorination of acetylene must contain the chloride anion, which participates in the reaction by activating the HCl molecule to form $[HCl_2]^-$. Notably, the structural modification of conjugated cations in ionic liquids is a key factor in improving the catalytic efficiency of acetylene. It is noted that the conversion achieved by ILs in this study, which is below 40%, still lags behind that of other metal-free catalysts.

Different from the previous dominant E–R mechanism for metal-free catalysts, a dual active site mechanism was proposed by Wang *et al.*[81] which utilized CaX molecular sieves loaded with imidazolyl il-1-ethyl-3-methylimidazolium tetrafluoroborate ([Emim][BF_4]) as catalysts for acetylene hydrochlorination, and revealed that the strong interactions between ionic liquids and zeolites can significantly enhance the catalytic performance. According to their study, the acetylene conversion of ILs/CaX was significantly increased with increasing temperature from 200 °C to 360 °C, and the optimum reaction temperature was determined to be 320 °C, with acetylene conversion close to 90% and VCM selectivity over 95%. Kinetic, TPD and IR spectroscopic analyses suggested that HCl adsorbed on Ca^{2+} in the zeolite reacted with acetylene adsorbed on ionic liquid cations to produce vinyl chloride, and the reaction order of C_2H_2 and HCl is 0.58 and 0.54 respectively as shown in Fig. 15c, and these observations corroborated the dual-site mechanism. Neither CaX nor [Emim][BF_4] has a good catalytic performance which signified the importance of interfacial sites between them during the reaction. Furthermore, DFT calculations revealed that the acetylene hydrochlorination reaction may first occur at the interface of ILs/CaX. A 200-minute-long stability test showed that acetylene conversion decreased from 46.5% to 16.3% while maintaining a VCM selectivity close to 95%. Finally, the IL/CaX catalyst was successfully regenerated by a simple vacuum operation, demonstrating its potential for sustainable utilization. In the end, ILs/CaX can deliver a STY of 0.75 kg_{VCM} (kg_{Cat} h)$^{-1}$ which is in the top tier for non-Au catalysts.

In order to conclude the general principle of ILs for acetylene hydrochlorination, four different quaternary phosphonium ILs (TPPB, TPPC, BuTPPB and TPPT) were synthesized by the incipient wet impregnation method by Nian *et al.*[109] They mainly investigated the effects of these ionic liquid cations and anions on the catalytic performance of the acetylene hydrochlorination reaction. DFT calculations indicated that all four ILs have strong adsorption capabilities towards HCl, specifically the calculated adsorption energy is −60.15 kJ mol^{-1}, −66.67 kJ mol^{-1}, −57.77 kJ mol^{-1}, and −41.13 kJ mol^{-1} for TPPB, TPPC, BuTPPB, and TPPT respectively. The strong adsorption of HCl is accompanied by a significant charge transfer from ILs to HCl. More interestingly, the adsorption of HCl is much stronger than the adsorption of both C_2H_2 and C_2H_3Cl; in particular the adsorption energy of C_2H_3Cl is well below −25 kJ mol^{-1} which facilitated the desorption. The calculated largest barrier in the pathway is 59.73 kJ mol^{-1}, 68.47 kJ mol^{-1}, 87.86 kJ mol^{-1} and 142.33 kJ mol^{-1} for TPPB, TPPC, BuTPPB, and TPPT, and is well correlated with the calculated HCl adsorption energy, and the bigger adsorption energy leads to a smaller barrier. The experimental test supported the predictions from DFT calculations. The initial conversions of C_2H_2 on the 15%TPPB/SAC, 15%TPPC/SAC, 15%BuTPPB/SAC and 15%TPPT/SAC catalysts were 84%, 81%,76% and 60%, respectively, which is consistent with the predicted reaction barrier from DFT. Further mechanism explored concluded that the effects of the anions on the catalytic activity were much significant than those of the cations, and IL catalysts mainly donated electrons to activate the H–Cl bond, and then, the electrons would be donated back to the IL catalyst in the transition state.

In another work from the same group,[83] the superior performance of TPPB was further investigated. They used spherical activated carbon (SAC) as a TPPB support and varied the loading amount from 0.5, 0.75 to 1.0 g to result in a series of TPPB/SAC catalysts. Under the condition of 180 °C and GHSV(C_2H_2) of 50 h^{-1}, 15% TPPB/SAC is identified as the best

performed catalyst with a C_2H_2 conversion of 83.7%, and the conversion can further increase to 95.9% when temperature is increased to 240 °C. The calculated TOF of 15% TPPB/SAC is determined to be 1.80 min^{-1}, which certified its superior intrinsic catalytic performance, and exceeded that of most of the recently reported metal-free catalysts as shown in Fig. 15d, and the stability of 15% TPPB/SAC is up to 300 h. 15% TPPB/SAC exhibited a strong adsorption of HCl and a weak adsorption of C_2H_2 and VCM as revealed from TPD analysis; DFT calculations revealed that the former has a binding energy of −14.39 kcal mol^{-1} and the latter have −5.47 and −4.09 kcal mol^{-1}. The electronic structure analysis confirmed that electrons are transferred from ILs to adsorbed HCl which caused the activation of the H–Cl bond and the largest barrier on the reaction pathway is determined to be 28.37 kcal mol^{-1} which is corresponding to the Cl addition to C_2H_3*.

Besides gas–solid catalysis, ILs have been examined as a mediator for acetylene hydrochlorination in a gas–liquid environment. Qin *et al.*[110] mixed ILs with various metal halides including $CuCl_2$, $SnCl_4$, $MnCl_4$, H_2PtCl_6 and $HAuCl_4$ as catalysts for acetylene hydrochlorination. From comparison, it is identified that [Bmim]Cl has the best performance among the investigated ILs, and it demonstrated 68.1% C_2H_2 conversion and 97.5% VCM selectivity at 160 °C coupled with $CuCl_2$. In the following, the authors carefully evaluated the influence of the C_2H_2/HCl ratio, space velocity, anion in ILs, and temperature. From the comparison, it is found that halogen anions such as Cl^{-1} and Br^{-1} showed much better performance than the other anions such as HSO_4^- and $PF6^-$. Under optimal conditions, $CuCl_2$/[Bmim]Cl exhibited 62.5% C_2H_2 conversion and 99% VCM selectivity, and the reactivity of catalysts did not show any decline over a 3 day test which indicated the superior durability.

The application of ILs in acetylene hydrochlorination opened a new route for green and sustainable development of catalysts. Meanwhile, ILs demonstrated unique properties which showed a clear difference from the other metal-free catalysts. In particular, ILs have a strong ability to activate HCl by electron donation which is rarely observed from other metal-free catalysts, and in turn caused the change of the reaction mechanism. Moreover, the rich combinations of various cations and anions provide a large space for IL optimization for acetylene hydrochlorination.

6. Conclusion and outlook

In this Feature Article, we have summarized the recent advances in metal-free materials as alternative catalysts to conventional metal-based catalysts in the hydrochlorination of acetylene, an important reaction in the traditional coal chemical industry. The rapid development of metal-free catalysts in acetylene hydrochlorination is one major impetus to provide this up-to-date summary which lays out a solid basis for the fast growing VCM industry in a sustainable and green manner. Carbon, boron nitride, graphitic C_3N_4, and ionic liquids, which have witnessed a great leap in both activity and stability, are selected for a meaningful comparison and discussion to reveal not only the difference from conventional metal catalysts but also the unique catalytic properties associated with each discussed metal-free material for acetylene hydrochlorination. Currently, the most studied metal-free catalysts for acetylene hydrochlorination are nitrogen doped carbon materials. Particularly, nitrogen doping has been widely explored because of its excellent conversion, selectivity, and stability as shown in Table 1. However, the active nitrogen species during reaction is still in debate and several nitrogen species including quaternary, pyridinic, and pyrrolic have been identified as the active site from diverse studies, which poses a great challenge for an on-purpose optimization of carbon catalysts. The catalytic role of the nitrogen dopant is suggested to activate the neighboring carbon which becomes the site for HCl/C_2H_2 adsorption. For nitrogen doped carbon catalysts, the reaction most likely obeys the E–R mechanism and the first step in the pathway is C_2H_2 adsorption due to the stronger adsorption of C_2H_2 than HCl. The deactivation of the catalyst is attributed to coke formation and the feasible regeneration methods such as NH_3 treatment could effectively restore the catalytic performance of nitrogen doped carbon catalysts. On the other hand, the performance of nitrogen doped carbon catalysts, in particular stability under industrial conditions such as high space velocity, is still lagging behind that of the contemporary metal-based catalysts. As indicated in the literature, the dual dopant strategy might be an option which could further boost the catalytic performance of doped carbon catalysts in acetylene hydrochlorination. The introduction of two different dopants could effectively modulate the binding strength of HCl and C_2H_2 which potentially changes the reaction mechanism and breaks the possible linear relationship between adsorption and the reaction barrier. In fact, the dual dopant methods have been widely used in other fields such as several key electrochemistry processes including HER, ORR, OER, *etc.*,[111,112] which gained substantial success for the metal-free carbon catalysts. Considering the rich combinations of kind and configuration between two dopants, there is a huge space for exploration; however the lack of the working principle for designing dual-dopant catalysts is a major obstacle which requires combined efforts from both experiment and computation.

Other than carbon materials, boron nitride, graphitic carbon nitride, and ionic liquids also demonstrated remarkable performance in acetylene hydrochlorination with their own catalytic character. Boron nitride perhaps exhibited the best catalytic performance of conversion and stability under relevant industrial conditions among the investigated metal-free materials, and DFT calculations suggested that carbon doping is an effective method to further increase the catalytic performance of boron nitride and the carbon dopant itself directly acted as the active site for reactant adsorption, which showed a different feature from the nitrogen dopant on carbon material. g-C_3N_4 provides a platform with high nitrogen content which showed a stronger adsorption of HCl than C_2H_2, and this is not found on both carbon and boron nitride catalysts. The adsorption preference directly caused a different reaction mechanism which is initiated by HCl adsorption. The most significant difference of ionic liquids from the other metal-free catalysts is the unique

dual-site L–H reaction mechanism because of the versatile cations and anions which are capable of delivering a balanced adsorption strength for HCl and C_2H_2, and it was found that the halogen anion is a guarantee for the good performance in acetylene hydrochlorination.

In the end, the rising of metal-free catalysts in acetylene hydrochlorination is eminent not only because of the strict environmental regulation and cost of metals but also because of their own excellent performance and durability which are well justified from the above discussions. However, there is a long way before the industrial implementation of metal-free catalysts which still require substantial improvements to meet the industrial standard. To our opinion, the most critical issue to be resolved for metal-free catalysts before industrial application is the durability under reaction conditions which significantly lags behind that of metal catalysts as shown in Table 1. As discussed before, coke formation and the collapse of the active structure are the main causes for deactivation of metal-free catalysts. For coke formation, the fine-tuning of properties of active sites to inhibit the side reaction could block the pathway for coke precursor formation, and hence reduce coke formation. Moreover, the optimization of morphology and pore structure could provide more space to accommodate coke which also extends the life of the catalyst. Regarding the collapse of the active structure, the composite configuration of different metal-free materials by chemical bonding coalescence is a good way to reinforce the mechanical stability. Besides, the synergetic effects induced by interfacial sites between different materials are also potentially conducive to improve performance. The application of external fields such as light and electricity could trigger the reaction under mild conditions which also benefits durability.

The current optimization strategy is still largely dependent on the trial-and-error methodology which is obviously less efficient. Therefore, not only well-designed new metal-free catalysts but also novel methods for optimization are equally urgently needed to further broaden the boundary and lift the blockage for rational improvements. Therefore, it is highly expected to see machine learning or Al powered methods to accelerate the process and pin down the hidden intrinsic relationship between structure and performance.[113] For this aspect, the cutting-edge large language models (LLMs) combined with machine learning could change the paradigm of catalyst design and discovery. The exceptional capability of LLMs to mine texts from thousands of literature resources could provide invaluable formatted data which can be utilized by machine learning to find the hidden relationship or optimal conditions for catalyst design, and this process is completely intractable for humans.[114,115] This methodology exactly meets the challenges of metal-free catalysts for industrial application due to the lack of clear guidelines for on-purpose optimization.

Overall, the transition from metal-based catalysts to the metal-free counterpart has begun in acetylene hydrochlorination and will change the landscape of this key reaction in the PVC industry.

Data availability

No primary research results, software or code have been included and no new data were generated or analysed as part of this review.

Conflicts of interest

There are no conflicts to declare.

Acknowledgements

This work was supported by the National Natural Science Foundation of China (Grant No. 22372105, 22172100), the Basic Research Project of Education Office of Liaoning Province (JYTZD2023183), the Fundamental Research Funds for the Liaoning Universities (LJ212410166043), ShenYang Normal University (BS202208) and The Program for Excellent Talents in Shenyang Normal University.

References

1 J. C. Davies, J. P. Miedziak, L. G. Bret and J. G. Hutchings, *Chin. J. Catal.*, 2016, **37**, 1600–1607.
2 M. Zhu, Q. Wang, K. Chen, Y. Wang, C. Huang, H. Dai, F. Yu, L. Kang and B. Dai, *ACS Catal.*, 2015, **5**, 5306–5316.
3 H. Xu and G. Luo, *J. Ind. Eng. Chem.*, 2018, **65**, 13–25.
4 W. F. Carroll, Jr., R. W. Johnson, S. S. Moore and R. A. Paradis, *Appl. Plast. Eng. Handb.*, 2017, 73–89.
5 L. Ye, X. Duan and S. Wu, *et al.*, *Nat. Commun.*, 2019, **10**, 914.
6 M. Conte, A. F. Carley, C. Heirene, D. J. Willock, P. Johnston, A. A. Herzing, C. J. Kiely and G. J. Hutchings, *J. Catal.*, 2007, **250**, 231–239.
7 J. Zhang, N. Liu, W. Li and B. Dai, *Front. Chem. Sci. Eng.*, 2011, **5**, 514–520.
8 J. Zhong, Y. Xu and Z. Liu, *Green Chem.*, 2018, **20**, 2412–2427.
9 H. Selin, *Global Environ. Polit.*, 2014, **14**, 1–19.
10 G. Malta, S. A. Kondrat and S. J. Freakley, *et al.*, *Science*, 2017, **355**, 1399–1403.
11 J. Zhang, W. Sheng, C. Guo and W. Li, *RSC Adv.*, 2013, **3**, 21062–21068.
12 J. Hu, Q. Yang, L. Yang, Z. Zhang, B. Su, Z. Bao, Q. Ren, H. Xing and S. Dai, *ACS Catal.*, 2015, **5**, 6724–6731.
13 J. Peng, D. Dong, Z. Wang, H. Yang, D. Qiao, Q. Wang, W. Sun, M. Liu, J. Wang, M. Zhu, B. Dai, F. He and C. Huang, *Nano Res.*, 2023, **16**, 9039–9049.
14 P. Johnston, N. Carthey and G. J. Hutchings, *J. Am. Chem. Soc.*, 2015, **137**, 14548–14557.
15 B. Nkosi, N. J. Coville and J. G. Hutchings, *Appl. Catal.*, 1988, **43**, 33–39.
16 J. G. Hutchings, *J. Catal.*, 1985, **96**, 292–295.
17 K. Zhou, J. Jia, C. Li, H. Xu, J. Zhou, G. Luo and F. Wei, *Green Chem.*, 2015, **17**, 356–364.
18 S. Mei, J. Gu, T. Ma, X. Li, Y. Hu, W. Li, J. Zhang and Y. Han, *Chem. Eng. J.*, 2019, **371**, 118–129.
19 W. Liu, M. Zhu and B. Dai, *New J. Chem.*, 2018, **42**, 20131–20136.
20 S. Chao, F. Zou, F. Wan, X. Dong, Y. Wang, Q. Guo, G. Wang and W. Li, *Sci. Rep.*, 2017, **7**, 39789.
21 Z. Chen, S. Wang, J. Zhao and R. Lin, *ACS Catal.*, 2024, **14**, 965–980.
22 X. Wang, W. Chen and X. Lei, *et al.*, *Coord. Chem. Rev.*, 2024, **500**, 215541.
23 S. Wei, G. Lan, Y. Qiu, D. Lin, W. Kong and Y. Li, *Chin. J. Catal.*, 2025, **70**, 8–43.
24 D. Su, S. Perathoner and G. Centi., *Chem. Rev.*, 2013, **113**, 5782–5816.
25 F. Rodriguez-Reinoso, *Carbon*, 1998, **36**, 159–175.
26 Y. Yang, K. Chiang and N. Burke, *Catal. Today*, 2011, **178**, 197–205.
27 I. Matos, M. Bernardo and I. Fonseca, *Catal. Today*, 2017, **285**, 194–203.
28 G. Lan, Y. Qiu, J. Fan, X. Wang, H. Tang, W. Han, H. Liu, H. Liu, S. Song and Y. Li, *Chem. Commun.*, 2019, **55**, 1430–1433.

29 A. G. Souza Filho, A. Jorio, G. G. Samsonidze, G. Dresselhaus, R. Saito and M. S. Dresselhaus, *Nanotechnology*, 2003, **14**, 1130.
30 Y. Qiu, S. Ali, G. Lan, H. Tong, J. Fan, H. Liu, B. Li, W. Han, H. Tang, H. Liu and Y. Li, *Carbon*, 2019, **146**, 406–412.
31 Y. Liu, H. Zhang, Y. Dong, W. Li, S. Zhao and J. Zhang, *Mol. Catal.*, 2020, **483**, 110707.
32 T. Liu, S. Ali, B. Li and D. S. Su, *ACS Catal.*, 2017, **7**, 3779–3785.
33 Y. Qiu, D. Fan, G. Lan, S. Wei, X. Hu and Y. Li, *Chem. Commun.*, 2020, **56**, 14877–14880.
34 Q. Tang, Y. Yue and Z. Jiang, *et al.*, *Catal. Commun.*, 2022, **167**, 106458.
35 F. Zhao and L. Kang, *ChemistrySelect*, 2017, **2**, 6016–6022.
36 Y. Fan, B. R. Goldsmith and P. G. Collins, *Nat. Mater.*, 2005, **4**, 906–911.
37 J. C. Charlier, *Acc. Chem. Res.*, 2002, **35**, 1063–1069.
38 L. Wang and M. Pumera, *Chem. Commun.*, 2014, **50**, 12662–12664.
39 Q. Xu, T. Kuang, Y. Liu, L. Cai, X. Peng, T. Sreeprasad, P. Zhao, Z. Yu and N. Li, *J. Mater. Chem. B*, 2016, **4**, 7204–7219.
40 T. Liu, S. Ali, Z. Lian, B. Li and D. S. Su, *J. Mater. Chem. A*, 2017, **5**, 21596–21603.
41 P. J. Paraknowitsch and A. Thomas, *Energy Environ. Sci.*, 2013, **6**, 2839–2855.
42 X. Li, J. Zhang, Y. Han, M. Zhu, S. Shang and W. Li, *J. Mater. Sci.*, 2018, **53**, 4913–4926.
43 J. Wang, W. Gong, M. Zhu and B. Dai, *Appl. Catal., A*, 2018, **564**, 72–78.
44 S. K. Kaiser, K. S. Song, S. Mitchell, A. Coskun and J. Pérez-Ramírez, *ChemCatChem*, 2020, **12**, 1922–1925.
45 X. Li, X. Pan and X. Bao, *J. Energy Chem.*, 2014, **23**, 131–135.
46 X. Li, X. Pan, L. Yu, P. Ren, X. Wu, L. Sun, F. Jiao and X. Bao, *Nat. Commun.*, 2014, **5**, 3688.
47 K. Zhou, B. Li, Q. Zhang, J. Q. Huang, G. L. Tian, J. C. Jia, M. Q. Zhao, G. H. Luo, D. S. Su and F. Wei, *ChemSusChem*, 2014, **7**, 723–728.
48 X. Li, Y. Wang, L. Kang, M. Zhu and B. Dai, *J. Catal.*, 2014, **311**, 288–294.
49 J. Zhao, J. Xu, J. Xu, T. Zhang, X. Di, J. Ni and X. Li, *Chem. Eng. J.*, 2015, **262**, 1152–1160.
50 R. Lin, S. K. Kaiser, R. Hauert and J. Pérez-Ramírez, *ACS Catal.*, 2018, **8**, 1114–1121.
51 B. Wang, Y. Yue, X. Pang, W. Zhu, Z. Chen, S. Shao, T. Wang, Z. Pan, X. Li and J. Zhao, *Phys. Chem. Chem. Phys.*, 2020, **22**, 20995–20999.
52 X. Qiao, X. Liu, Z. Zhou, Q. Guan and W. Li, *Catal. Sci. Technol.*, 2021, **11**, 2327–2339.
53 X. Li, P. Li, X. Pan, H. Ma and X. Bao, *Appl. Catal., B*, 2017, **210**, 116–120.
54 F. Lu, Q. Wang, M. Zhu and B. Dai, *Molecules*, 2023, **28**, 956.
55 A. P. Van Trimpont, B. G. Marin and F. G. Froment, *Appl. Catal.*, 1985, **17**, 161–173.
56 Y. Yue, B. Wang, S. Wang, C. Jin, J. Lu, Z. Fang, S. Shao, Z. Pan, J. Ni, J. Zhao and X. Li, *Chem. Commun.*, 2020, **56**, 5174–5177.
57 R. Chang, G. Cheng and T. Feng, *et al.*, *ACS Catal.*, 2024, **14**, 16687–16697.
58 X. Qi, W. Chen and J. Zhang, *RSC Adv.*, 2020, **10**, 34612–34620.
59 S. Wang, Z. Liu and D. Xu, *et al.*, *Mol. Catal.*, 2024, **563**, 114240.
60 Z. Guo, W. Peng, J. Li, F. Li, Q. Zhang, L. Yang, D. Xie, Y. Dong, J. Zhang and H. Zhang, *New J. Chem.*, 2023, **47**, 14019–14029.
61 Z. Shen, P. Xing, K. Wen and B. Jiang, *Catalysts*, 2023, **13**, 432.
62 S. Wei, Y. Qiu, X. Sun, X. Wang, H. Li, G. Lan, J. Liu and Y. Li, *ACS Sustainable Chem. Eng.*, 2022, **10**, 10476–10485.
63 F. Li, H. Zhang, M. Zhang, W. Peng, L. Yao, Y. Dong and J. Zhang, *Mol. Catal.*, 2022, **527**, 112405.
64 F. Lu, D. Xu, Y. Lu, B. Dai and M. Zhu, *Chin. J. Chem. Eng.*, 2021, **29**, 196–203.
65 Y. Liu, H. Zhang, X. Li, L. Wang, Y. Dong, W. Li and J. Zhang, *Appl. Catal., A*, 2021, **611**, 117902.
66 X. Tao, F. Chen, Y. Xie, X. Cheng, X. Liu and G. Gao, *J. Taiwan Inst. Chem. Eng.*, 2021, **126**, 80–87.
67 Z. Shen, Y. Liu, Y. Han, Y. Qin, J. Li, P. Xing and B. Jiang, *RSC Adv.*, 2020, **10**, 14556–14569.
68 Y. Lu, F. Lu and M. Zhu, *J. Taiwan Inst. Chem. Eng.*, 2020, **113**, 198–203.
69 F. Lu, Y. Lu, M. Zhu and B. Dai, *ChemistrySelect*, 2020, **5**, 878–885.
70 X. Liu, X. Qiao, Z. Zhou, C. Zhao, Q. Guo and W. Li, *Catal. Commun.*, 2020, **147**, 106147.
71 X. Qiao, Z. Zhou, X. Liu, C. Zhao, Q. Guan and W. Li, *Catal. Sci. Technol.*, 2019, **9**, 3753–3762.
72 X. Qiao, C. Zhao, Z. Zhou, Q. Guan and W. Li, *ACS Sustainable Chem. Eng.*, 2019, **7**, 17979–17989.
73 G. Lan, Y. Wang, Y. Qiu, X. Wang, J. Liang, W. Han, H. Tang, H. Liu, J. Liu and Y. Li, *Chem. Commun.*, 2018, **54**, 623–626.
74 Y. Yang, G. Lan, X. Wang and Y. Li, *Chin. J. Catal.*, 2016, **37**, 1242–1248.
75 X. Wang, B. Dai, Y. Wang and F. Yu, *ChemCatChem*, 2014, **6**, 2339–2344.
76 X. Li, Y. Wang, L. Kang, M. Zhu and B. Dai, *J. Catal.*, 2014, **311**, 288–294.
77 F. Lu, C. Wei, X. Yin, K. Li, M. Zhu and B. Dai, *Nanomaterials*, 2022, **12**, 2619.
78 X. Dong, G. Liu, Z. Chen, Q. Zhang, Y. Xu and Z. Liu, *Mol. Catal.*, 2022, **525**, 112366.
79 Z. Shen, Y. Liu, Y. Han, Y. Qin, J. Li, P. Xing and B. Jiang, *RSC Adv.*, 2020, **10**, 14556–14569.
80 Y. Yue, *et al.*, *Chem. Commun.*, 2020, **56**, 5174–5177.
81 B. Wang, H. Lai and Y. Yue, *et al.*, *Catalysts*, 2018, **8**, 351.
82 X. Zhou, S. Xu, Y. Liu and S. Cao, *Mol. Catal.*, 2018, **461**, 73–79.
83 X. Li, Y. Nian, S. Shang, H. Zhang, J. Zhang, Y. Han and W. Li, *Catal. Sci. Technol.*, 2019, **9**, 188–198.
84 P. Li, H. Li, X. Pan, K. Tie, T. Cui, M. Ding and X. Bao, *ACS Catal.*, 2017, **7**, 8572–8577.
85 X. Qi, W. Chen and J. Zhang, *RSC Adv.*, 2019, **9**, 21931–21938.
86 J. Li, G. Lan, L. Zhi, H. Liu and Y. Li, *Ind. Catal.*, 2017, 1008–1043.
87 G. J. Hutchings, *J. Catal.*, 1985, **96**, 292–295.
88 J. Pérez-Ramírez and N. López, *Nat. Catal.*, 2019, **2**, 971–976.
89 S. Bag, B. Mondal, A. K. Das and C. R. Raj, *Electrochim. Acta*, 2015, **163**, 16–23.
90 B. Dai, K. Chen, Y. Wang, L. Kang and M. Zhu, *ACS Catal.*, 2015, **5**, 2541–2547.
91 J. Wang, F. Zhao, C. Zhang, L. Kang and M. Zhu, *Appl. Catal., A*, 2018, **549**, 68–75.
92 X. Dong, S. Chao, F. Wan, Q. Guan, G. Wang and W. Li, *J. Catal.*, 2018, **359**, 161–170.
93 J. Zhao, B. Wang, Y. Yue, G. Sheng, H. Lai, S. Wang, L. Yu, Q. Zhang, F. Feng, Z. T. Hu and X. Li, *J. Catal.*, 2019, **373**, 240–249.
94 A. Li, D. Tian and Z. Zhao, *New J. Chem.*, 2020, **44**, 11584–11592.
95 H. Li, J. Zhang, P. Wu, S. Xun, W. Jiang, M. Zhang, W. Zhu and H. Li, *J. Phys. Chem. C*, 2019, **123**, 2256–2266.
96 Z. Zhang, J. Tian, X. Wu, I. Surin, J. Pérez-Ramírez, P. Hemberger and A. Bodi, *J. Am. Chem. Soc.*, 2023, **145**, 7910–7917.
97 H. Tian, W. Li, L. He, Y. Zhong, S. Xu, H. Xiao and N. Xu, *Nat. Commun.*, 2023, **14**, 6520.
98 J. T. Grant, C. A. Carrero, F. Goeltl, J. Venegas, P. Mueller, S. P. Burt, S. E. Specht, W. P. McDermott, A. Chieregato and I. Hermans, *Science*, 2016, **354**, 1570–1573.
99 X. Wei, M. S. Wang, Y. Bando and D. Golberg, *ACS Nano*, 2011, **5**, 2916–2922.
100 C. Si, Z. Lian, M. Yang and B. Li, *Appl. Surf. Sci.*, 2021, **566**, 150710.
101 Q. Wang, G. Fan, H. Xu, X. Tu, X. Wang and X. Chu, *Mol. Catal.*, 2020, **488**, 110853.
102 F. Zhao, Y. Wang, M. Zhu and L. Kang, *RSC Adv.*, 2015, **5**, 56348–56355.
103 P. Niu, M. Qiao, Y. Li, L. Huang and T. Zhai, *Nano Energy*, 2018, **44**, 73–81.
104 H. Yu, R. Shi and Y. Zhao, *et al.*, *Adv. Mater.*, 2017, **29**, 1605148.
105 N. Sahiner, A. O. Yasar and N. Aktas, *Renewable Energy*, 2017, **101**, 1005–1012.
106 W. Zhang, Q. Wang, H. Wu, P. Wu and M. He, *Green Chem.*, 2014, **16**, 4767–4774.
107 M. J. Schneider, M. Lijewski, R. Woelfel, M. Haumann and P. Wasserscheid, *Angew. Chem.*, 2013, **125**, 7134–7137.
108 F. Pöhlmann, L. Schilder, W. Korth and A. Jess, *ChemPlusChem*, 2013, **78**, 570–577.
109 Y. Nian, J. Zhang, X. Li, Y. Wang, W. Li, P. D. Kolubah and Y. Han, *Phys. Chem. Chem. Phys.*, 2019, **21**, 7635–7644.
110 G. Qin, Y. Song, R. Jin, J. Shi, Z. Yu and S. Cao, *Green Chem.*, 2011, **13**, 1495–1498.
111 Q. Wang, Y. Ji, Y. Lei, Y. Wang, Y. Wang, Y. Li and S. Wang, *ACS Energy Lett.*, 2018, **3**, 1183–1191.
112 K. Jiang and H. Wang, *Chem*, 2018, **4**, 194–195.
113 T. Ansari and S. Taqvi, *ChemBioEng Rev.*, 2023, **10**, 884–906.
114 G. Lei, R. Docherty and S. J. Cooper, *Digital Discovery*, 2024, **3**, 1257–1272.
115 M. Schilling-Wilhelmi, M. Ríos-García, S. Shabih, M. V. Gil, S. Miret, C. T. Koch, J. A. Marquez and K. M. Jablonka, *Chem. Soc. Rev.*, 2025, **54**, 1125–1150.